TABLE OF CONTENTS


| | | Page | |
|---|---|---|---|
| | SUMMARY | 1 | 1/A6 |
| | SYMBOLS | 1 | 1/A6 |
| I. | INTRODUCTION | 2 | 1/A7 |
| II. | SIMULATION STRATEGY | 5 | 1/A10 |
| | A. Spatial and Temporal Location of Individual Pressure Events | 5 | 1/A10 |
| | B. Frequency Associated with Pressure Fluctuation Event | 6 | 1/A11 |
| | C. Amplitude of Individual Pressure Events | 6 | 1/A11 |
| | D. Construction of a Convected Sequence of Pressure Events | 6 | 1/A11 |
| III. | EVALUATION AND OPTIMIZATION OF PRESSURE SIMULATION | 9 | 1/A14 |
| | A. Wave Form | 20 | 1/B11 |
| | B. Frequency-Generating Function | 23 | 1/B14 |
| | C. Frequency-Dependent Decay | 25 | 1/C2 |
| IV. | RESULTS AND DISCUSSION | 28 | 1/C5 |
| | APPENDIX: PRESSURE SIMULATION FORTRAN PROGRAM | 31 | 1/C8 |
| | REFERENCES | 39 | 1/D2 |


LIST OF TABLES


| Table | | | |
|---|---|---|---|
| 1 | Carrier wave models | 13 | 1/B4 |

LIST OF FIGURES


| Figure | | Page | |
|---|---|---|---|
| 1 | Probability distribution of time between bursts . . . . . | 7 | 1/A12 |
| 2 | Power spectrum generated by simulation from reference 13 . . . . . | 10 | 1/B1 |
| 3 | Space-time correlation by simulation from reference 13 . . . . . | 11 | 1/B2 |
| 4 | Composite spectrum for various wave forms . . | 14 | 1/B5 |
| 5 | Space-time correlation for the double sine wave simulation . . . . . | 15 | 1/B6 |
| 6 | Space-time correlation for the eighth power wave simulation . . . . . | 16 | 1/B7 |
| 7 | Space-time correlation for jitter wave simulation . . . . . | 17 | 1/B8 |
| 8 | Space-time correlation for skewed wave simulation . . . . . | 18 | 1/B9 |
| 9 | Wall pressure power spectrum for sinusoidal disturbances, decay varying linearly with frequency . . . . . | 21 | 1/B12 |
| 10 | Space-time correlation for sinusoidal waves with decay a linear function of frequency . . | 22 | 1/B13 |
| 11 | Modified power spectrum and cumulative probability required for frequency generator . . . . . | 24 | 1/C1 |
| 12 | Power spectrum after optimization . . . . . | 26 | 1/C3 |
| 13 | Space-time correlation after optimization . . | 27 | 1/C4 |

NASI.26:2958

MAY 26 1978

NASA Contractor Report 2958

COMPLETED
ORIGINAL

# Simulation of Turbulent Wall Pressure

Robert L. Ash

GRANT NSG-1100
MAY 1978

NASA

46

NAS1.26:2958

NASA Contractor Report 2958

# Simulation of Turbulent Wall Pressure

Robert L. Ash
*Old Dominion University*
*Norfolk, Virginia*

**Prepared for**
**Langley Research Center**
**under Grant NSG-1100**

National Aeronautics
and Space Administration

**Scientific and Technical**
**Information Office**

**1978**

BLANK PAGE

## SUMMARY

A Monte Carlo procedure has been developed to simulate turbulent boundary layer wall pressure fluctuations. The approach utilizes much of the newly available conditional sampling information to construct the required distribution functions. Various disturbance wave forms have been examined, as well as the effect of frequency-dependent decay. Good agreement between the simulation and experimental data has been achieved for root mean square pressure level, power spectrum, and space-time correlation.


## SYMBOLS

| | |
|---|---|
| $f$ | frequency (Hz) |
| $n$ | random number |
| $p$ | pressure |
| $p_{rms}$ | root mean square pressure |
| $R_{pp}$ | space-time correlation |
| $S_t$ | Strouhal number ($\omega\ \delta^*/U_\infty$) |
| $T$ | integration time interval |
| $t$ | time |
| $t_o$ | reference time |
| $U_\infty$ | free stream velocity |

| | |
|---|---|
| $u_c$ | convection velocity |
| $u_\tau$ | friction velocity |
| $x$ | coordinate in direction of flow |
| $x_D$ | development length |
| $y$ | transverse coordinate |
| $\gamma$ | frequency adjustment parameter |
| $\delta^*$ | displacement thickness |
| $\nu$ | kinematic viscosity |
| $\tau$ | dimensionless time ($U_\infty t/\delta^*$) |
| $\tau_w$ | wall shear stress |
| $\omega$ | radian frequency |

## I. INTRODUCTION

The purpose of this report is to present a procedure for simulating wall pressure fluctuations beneath a low speed, fully turbulent boundary layer. A simulation was desired because it could supply local pressure fluctuation data with arbitrary spatial and temporal resolution for a variety of velocity and boundary layer thickness conditions. The arbitrary resolution feature permits direct coupling between simulated boundary layer pressure fluctuations and numerical structural analysis codes, resulting in straightforward prediction of local surface motion produced by the simulated turbulent boundary layer. This work represents part of a compliant wall drag reduction study undertaken at NASA/Langley Research Center.

Bushnell, Hefner, and Ash (ref. 1) have discussed a possible mechanism for reducing skin friction drag by means of a compliant surface. Based on that discussion, it is apparent that such an effect can exist only if the surface motion is compatible with the turbulent flow structure. They have suggested that the violent turbulent "bursts" near the wall, as discussed by Offen

and Kline (ref. 2), can be inhibited by a suitable periodic surface motion. In addition to the connection between surface motion and inner turbulent flow structure, it is known that the wall pressure fluctuations are produced primarily by large vorticular structures in the outer portion of the boundary layer (see Praturi, ref. 3, for a description of the outer flow structures). Consequently, the surface motion is driven by disturbances emanating from the outer part of the boundary layer, and is required to interact with flow structures in the inner region. These conditions put stringent requirements on wall pressure simulation and surface motion calculations. Ash and Balasubramanian (ref. 4) have discussed some of those problems. It should be evident that the simulation of turbulent wall pressure fluctuations must be connected as closely as possible to the physics of the flow. Furthermore, the simulated turbulent structure must result in pressure fluctuation statistics that reproduce accepted experimental data.

Willmarth (ref. 5) has summarized most of the experimental measurements of turbulent wall pressure statistics, and only those measurements which were needed for the simulation are mentioned here. Willmarth and Woolridge (ref. 6) and Bull (ref. 7) have presented detailed measurements of wall pressure energy spectra and space-time correlations. Both investigations found that the pressure energy spectrum peaked at a Strouhal number ($S_t = \omega\ \delta^*/U_\infty$) of about 0.2, that the root mean square pressure was related to the wall shear stress ($p_{rms} \simeq 2.5$ to $2.8\ \tau_w$), and that pressure fluctuations were convected downstream with varying speeds. They were uncertain whether the pressure disturbances with different sizes (or frequencies) were convected with different velocities, or whether disturbances actually changed speeds, or both. Both investigations did reveal more rapid decay in the correlation of high frequency pressure fluctuations than low frequency fluctuations. Emmerling (ref. 8) used an optical method to simultaneously measure pressure fluctuations on a rectangular area. His measurements confirmed the previously observed wide variation in convection speeds, but he also found that root mean square pressure levels were strong functions of the diameter of the

pressure sensor. However, Bull and Thomas (ref. 9) suggest that a significant portion of the pressure discrepancy is due to the type of pressure sensor used in those experiments. Bull and Thomas' measurements did confirm a modest increase in rms pressure levels with decreasing sensor diameters. Burton (ref. 10) has utilized conditional sampling techniques to relate instantaneous wall pressure data to the structural features of the turbulent flow. He found that "bursts" (see Offen and Kline, ref. 2), which are a major source of Reynolds stresses at the wall, are highly correlated with the occurrence of large instantaneous, local adverse pressure gradients. Burton was unable to link the burst structure with the development of the outer structure of the turbulent flow.

The present work is not the first attempt to calculate numerically turbulent wall pressure. Deardorff (ref. 11) used a finite difference solution to the Navier-Stokes equations for flow in a channel to calculate pressure fluctuations. That work has been extended by Schumann (ref. 12) for an annular flow. Both were able to show good agreement between their computed rms pressure levels and experiments. However, because of computational limitations on spatial resolution and time step, neither was capable of simulating energy spectra or space-time correlations. Although the Navier-Stokes solution approach is clearly the most fundamentally correct method for calculating turbulent wall pressure fluctuations, it is currently incapable of resolving that data sufficiently to produce detailed statistical approximations to the experimental data. The method employed here attempts to simulate the structural features of a turbulent boundary layer as observed in experimental measurements, and does not attempt to satisfy the equations of motion. Rather, it is anticipated that the simulated wall pressure might be useful in conjunction with Navier-Stokes solvers by providing a realistic dynamic pressure boundary condition.

## II. SIMULATION STRATEGY

Ash (ref. 13) has discussed the preliminary strategy employed in this work. Essentially, single cycle pressure fluctuations are convected over a model surface, and their contribution to the local instantaneous pressure field is stored at user-specified spatial locations with a user-specified time resolution. A Monte Carlo method has been used to locate the origin of each pressure fluctuation event (both spatial location and time), as well as to assign frequency and amplitude. The basis for the various distribution functions used in the Monte Carlo approach will be discussed here.

### A. Spatial and Temporal Location of Individual Pressure Events

Burton (ref. 10) has shown that the bursts in the near wall flow are highly correlated with the wall pressure. Regardless of whether the burst structures evolve into the large outer structure of the boundary layer or not, the burst data represents a good measure of distance and time between individual pressure fluctuation events. Offen and Kline (ref. 2) indicate that spatial separation, $\Delta x$, and temporal separation, $\Delta t$, between burst events are related by

$$\Delta x = u_\tau \, \Delta t$$

or

$$\Delta x = \delta^* \frac{u_\tau}{U_\infty} \Delta \tau \ , \qquad (1)$$

where $u_\tau$ is the friction velocity, $\delta^*$ is the displacement thickness, $U_\infty$ is the free stream velocity, and $\tau$ is dimensionless time ($\tau = U_\infty t/\delta^*$).

Burst occurrence measurements from Offen and Kline (ref. 2) have been used to construct the probability density function

shown in figure 1. From that figure it can be seen that a Gamma distribution represents the data reasonably well. Ash (ref. 13) has shown that the cumulative probability distribution, constructed from the Gamma distribution, is well represented by the Monte Carlo distribution function:

$$\tau = 32.2 - \frac{2}{n + 0.619} + 72\, n^2 + 0.63 \tan \frac{\pi}{2} n \qquad (2)$$

where $n$ is a uniformly distributed ($0 \leq n \leq 1$) random number.

Equations (1) and (2) can also be used to assign the distance between pressure events, since $\tau$ is actually $\Delta\tau$ -- the temporal separation between events.

B. Frequency Associated with Pressure Fluctuation Event

Bull's (ref. 7) power spectrum measurements have been used as a basis for constructing the frequency-generating function. As reported by Ash (ref. 13) a cumulative probability function can be constructed from the power spectrum. However, the individual, single cycle pressure disturbances so generated do not necessarily reproduce the prescribed power spectrum. Problems of that type encountered in this investigation will be discussed subsequently.

C. Amplitude of Individual Pressure Events

Because of the triggering strategy used in Burton's (ref. 10) conditional sampling measurements, it has been possible to infer that the distribution of individual pressure event amplitudes is Gaussian. Obviously, the mean level is zero and the standard deviation is simply the root mean square pressure.

D. Construction of a Convected Sequence of Pressure Events

As the individual pressure events are convected downstream, their amplitude must decay. Bull (ref. 7) has measured the decay rate, and it is well approximated by

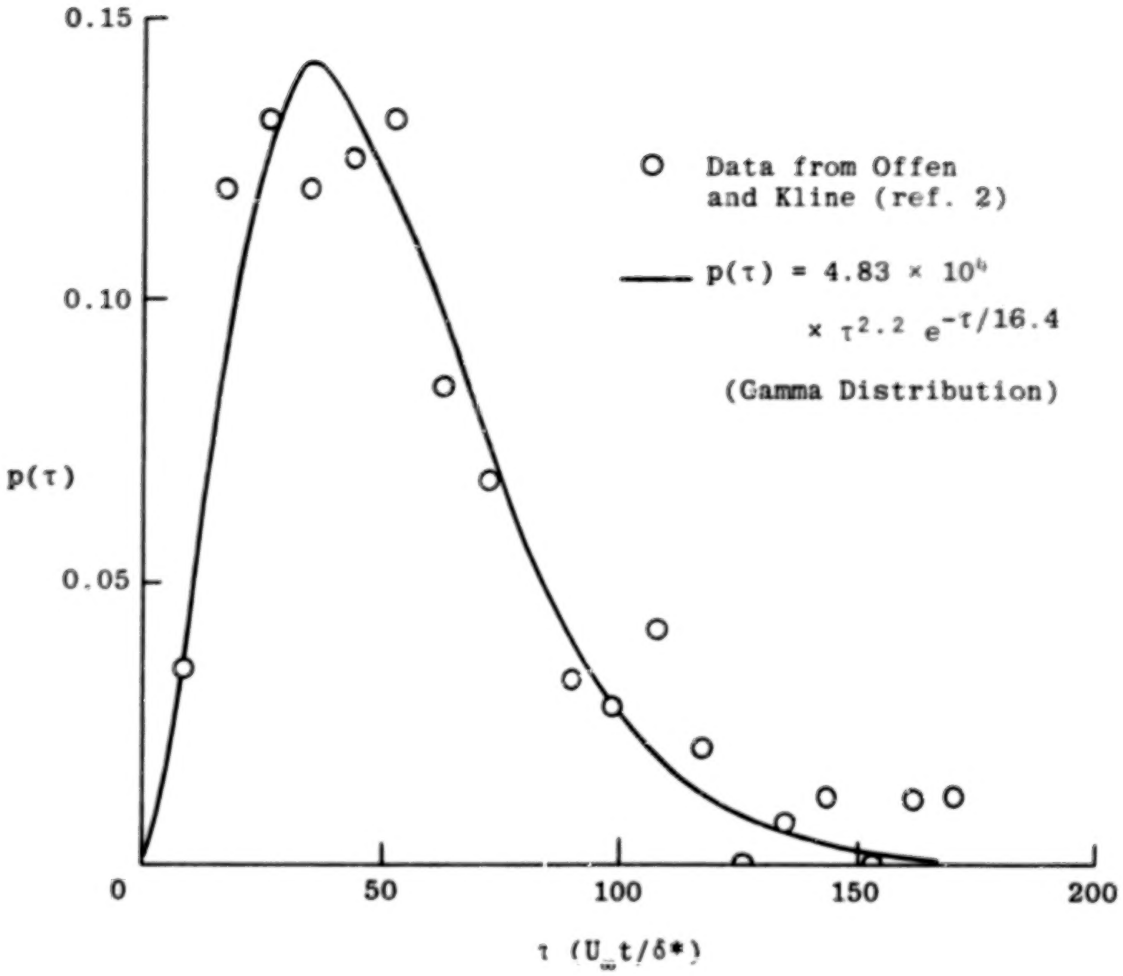


**Figure 1. Probability distribution of time between bursts.**

$$|p(x + x_o)|/|p(x_o)| = 1 - e^{-4260\ \nu/(u_\tau x)} \tag{3}$$

where $|p(x + x_o)|$ is the amplitude of the disturbance at a distance $x$ from its original location. The above equation does not account for frequency-dependent decay.

Although a substantial amount of evidence indicates that disturbances are convected downstream with a range of speeds $\left(0.5 \leq \frac{u_c}{U_\infty} \leq 0.85\right)$, a constant and relatively high value of

$$u_c = 0.8\ U_\infty \tag{4}$$

has been used here. There appear at this time to be no measurements which relate convection speed to size and location of pressure disturbances.

At this point, spatial and temporal spacing, frequency, amplitude, decay rate, and convection speed models have been discussed. The only remaining features are the procedure for constructing an orderly progression of pressure events and a determination of the required development length for startup of the simulation.

Obviously, the required model development length can be determined using the spatial decay equation. If one assumes that disturbances which have decayed to an amplitude of one percent of their original value are negligible, the required startup, $x_D$, is given by

$$x_D = 0.425 \times 10^6\ u_\tau/\nu \tag{5}$$

from equation (3).

The sequence of pressure disturbances is constructed by employing equations (1) and (2) along with a random number generator to march from the leading edge of the development length to the trailing edge of the model (region over which pressure is recorded). The distance between event birth locations is thus random and

distributed in a manner consistent with Offen and Kline's (ref. 2) burst data. A reference time, $t_o$, is frozen during the random $\Delta x$ travel from leading edge to trailing edge, but the time of birth of each event, $\Delta t_n$, is distributed away from $t_o$ by

$$t_{birth} = t_o + \Delta t_n \quad , \tag{6}$$

again, using equation (2) and a random number generator for $\Delta t_n$. Each $\Delta t_n$ is stored during the spatial travel from leading to trailing edge, and an average time step, $\Delta t_{avg}$, is computed for each complete spatial excursion. A new reference time, $t_c = t_o + \Delta t_{avg}$, is then used, and the procedure is repeated. As each pressure event is convected over the desired storage locations, its contribution is stored at user-specified time intervals.

Further details of the initial development of this procedure are given in Ash, reference 13. At that time, only rms pressure level and a pressure signal had been produced. The statistical features of the simulation had not been examined, and no attempt had been made to optimize the simulation. A detailed study of the various factors which influence the quality of the pressure simulation has been carried out since that time.

## III. EVALUATION AND OPTIMIZATION OF PRESSURE SIMULATION

Initially, a single period, sine wave was employed to carry the pressure fluctuation event information. The power spectrum resulting from the simulation just described is shown in figure 2. The space-time correlation, defined by

$$R_{pp}\left(\frac{x}{\delta^*},\ \tau\right) = \frac{\frac{1}{T}\int_o^T p(0,t)\ p\left(\frac{x}{\delta^*},\ t+\tau\right)dt}{p_{rms}(0)\ p_{rms}\left(\frac{x}{\delta^*}\right)} \tag{7}$$

is shown in figure 3, along with Bull's (ref. 7) measurements. Neither of the simulated results was satisfactory.

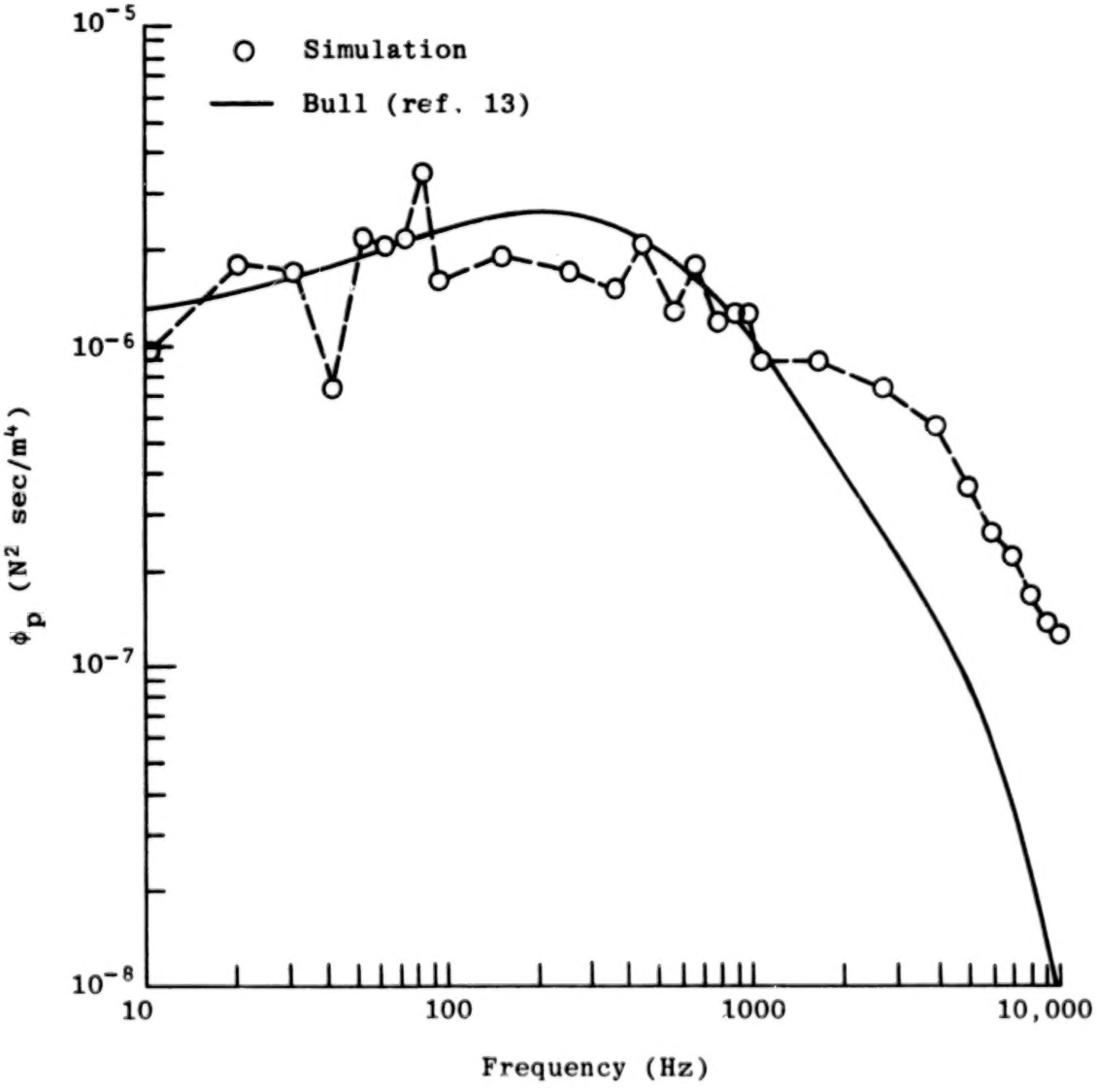


Figure 2. Power spectrum generated by simulation from reference 13.

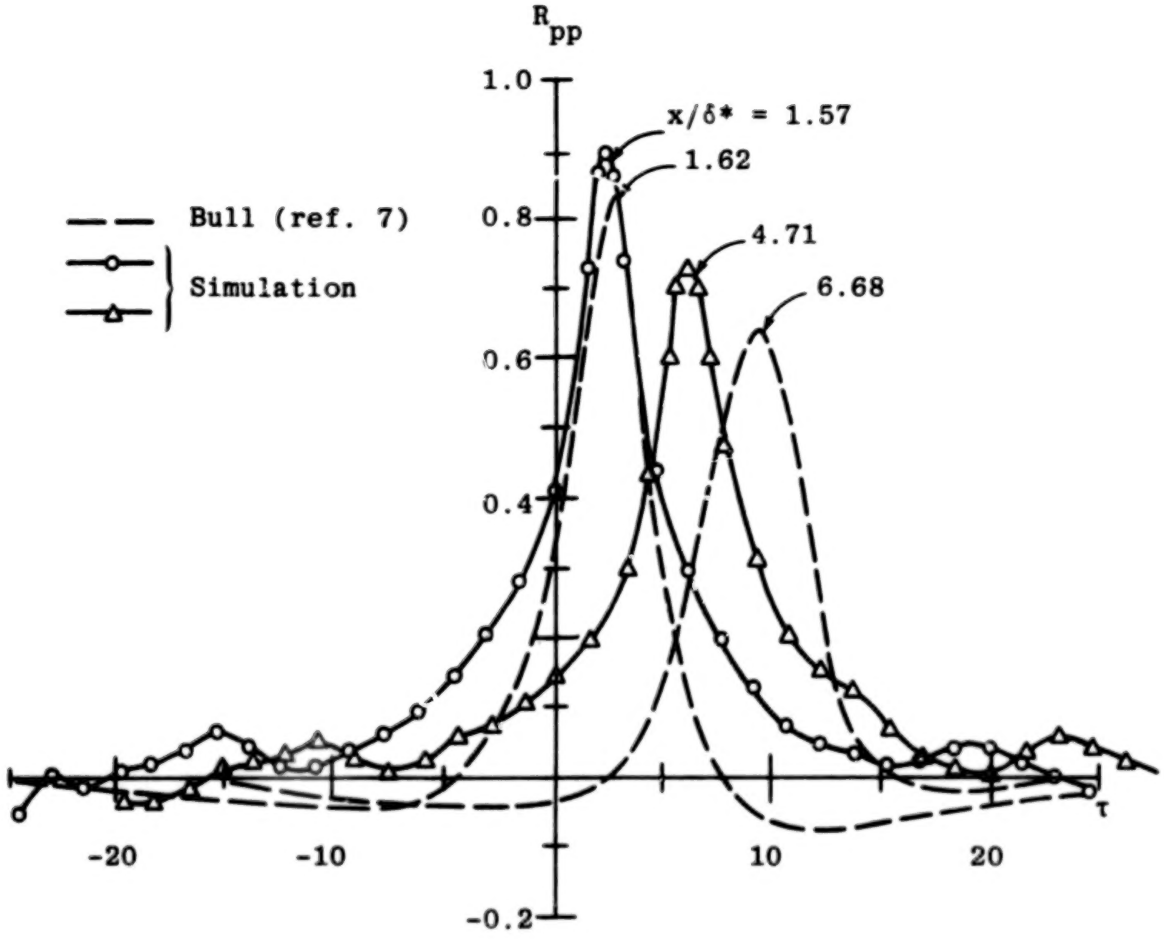


Figure 3. Space-time correlation by simulation from reference 13.

Since there was no physical basis for employing a simple sine wave as the pressure event carrier, an investigation of other wave shapes was undertaken. Four other wave shapes were examined. Their names (for reference purposes) and equations are given in table 1, along with a sketch of the wave form. A composite power spectrum for all five waves (including the original sine wave) is shown in figure 4. Except at low frequencies where the spectral resolution is not very good (resulting in data scatter), little effect of wave shape can be observed on the power spectrum.

Comparison of the space-time correlations with Bull's (ref. 7) data are shown in figures 5 through 8. It is evident from figure 5 that the double sine wave affects significantly the space-time correlation. Very good agreement in shape and width of positive correlation between Bull's data and the simulation has been achieved. At $x/\delta^*$ of 6.28, the correlation is too narrow at its peak, but remains in good qualitative agreement. All other wave forms (figures 3 and 6 through 8) show varying degrees of agreement. Significantly, only the double sine wave carrier caused the space-time correlation to possess the negative correlation regions observed in Bull's (ref. 7) measurements. Discrepancies in the correlation peaks were not considered significant because they could be adjusted by changing the constant in equation (3).

The wave form investigation was expected to accomplish two things. First, it was desired to select a carrier wave which would yield space-time correlations which were comparable to the experimental measurements. Secondly, it was hoped that one or more of the wave forms would yield spectral distributions closer to the experimental measurements. The second phase was not successful per se, but led to two other observations. Not only was the power spectrum nearly insensitive to the wave forms examined, but wave shapes which were very similar to the double sine wave did not produce similar space-time correlations.

Two important features of the experimental measurements of Bull (ref. 7) and Willmarth and Woolridge (ref. 6) had not been modeled at this point. Both investigations suggested that

Table 1. Carrier wave models.

| Name | Equation | Shape | Symbol |
|---|---|---|---|
| Sine | $\sin\theta$ | 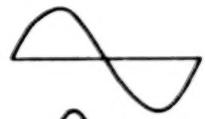 | ○ |
| Double Sine | $\sin\theta - \frac{1}{2}\sin 2\theta$ | | □ |
| Eighth Power | $\sin\theta\left(1 - \cos^8\frac{\theta}{2}\cos\theta\right)$ | 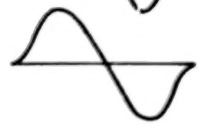 | ◇ |
| Jitter | $100\left[\sin\theta - .5314\sin\frac{\theta + .05\pi}{1.05} - .4812\sin\frac{\theta + .05\pi}{.95}\right]$ | | △ |
| Skewed | $14.4\left[\sin\theta - .5005\sin\frac{\theta + 2\pi}{1.05} - .5513\sin\frac{\theta + 2\pi}{.95}\right]$ | | ⌂ |

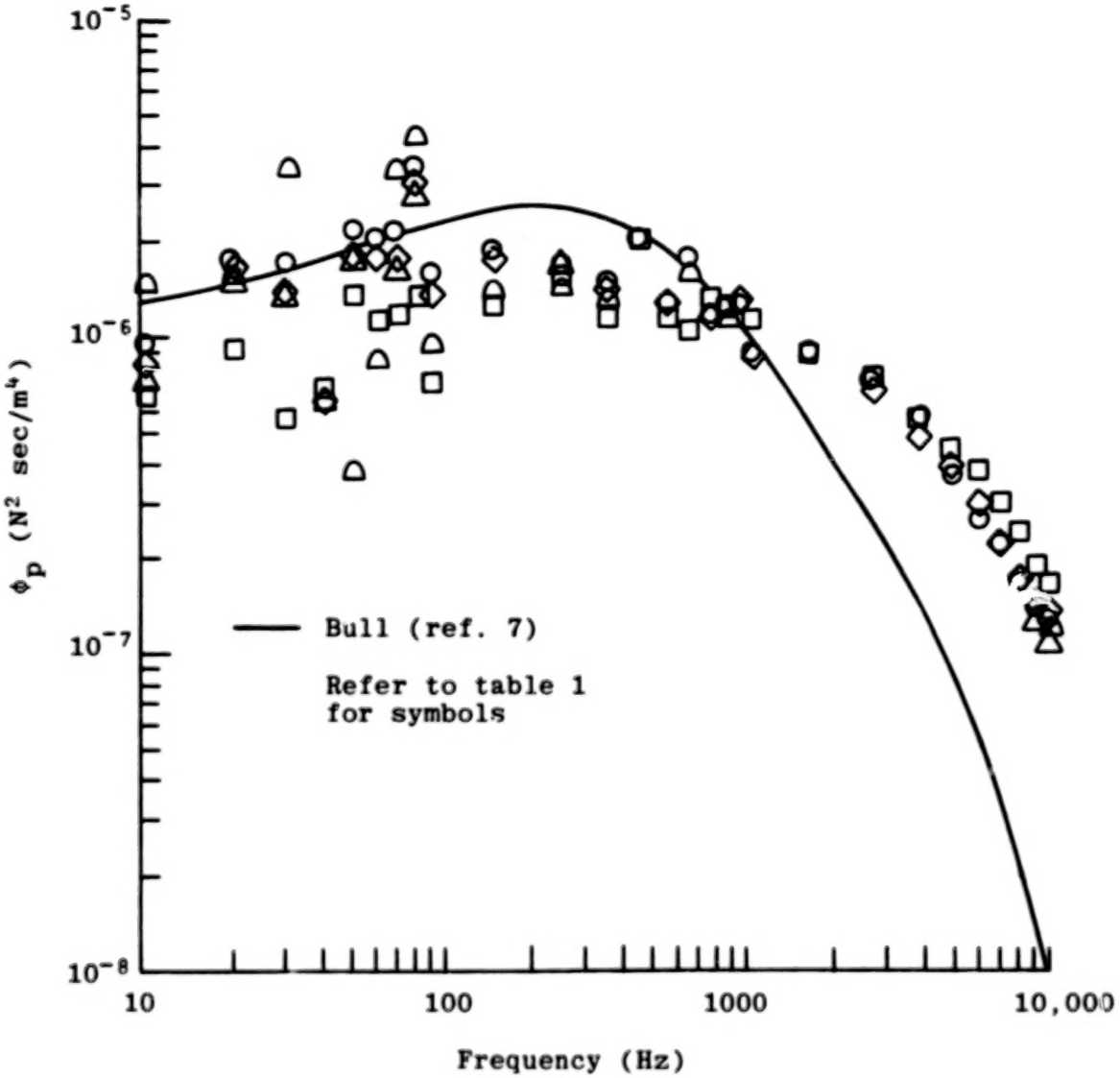


Figure 4. Composite spectrum for various wave forms.

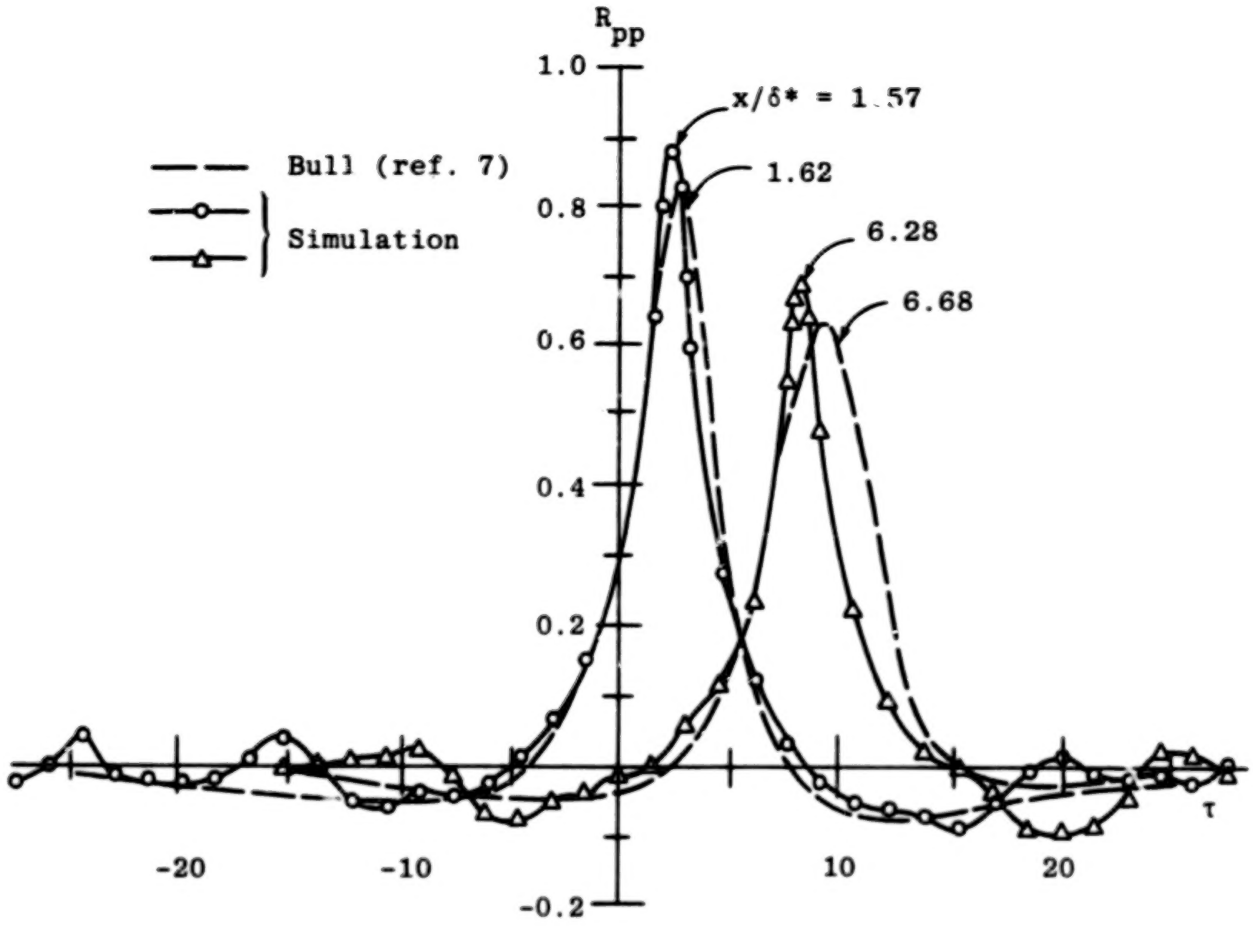


Figure 5. Space-time correlation for the double sine wave simulation.

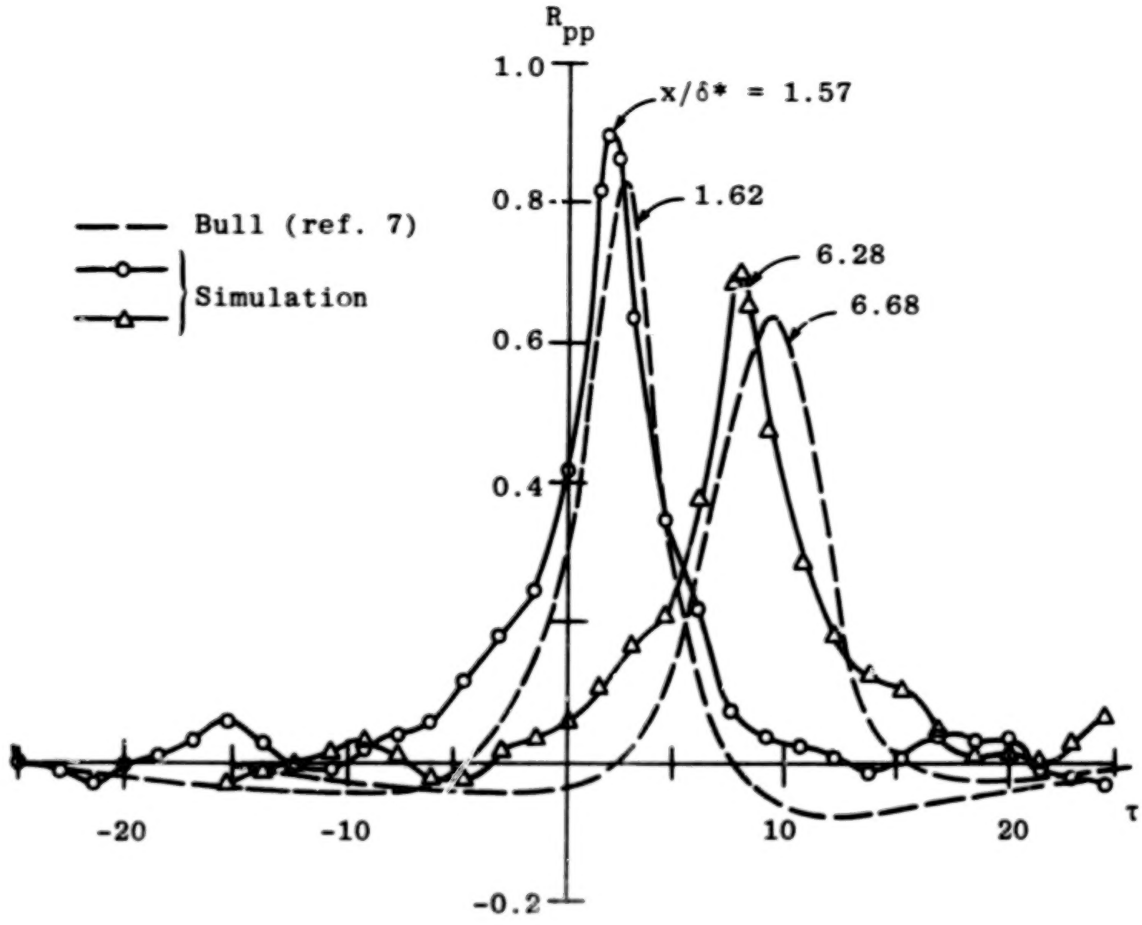


Figure 6. Space-time correlation for the eighth power wave simulation.

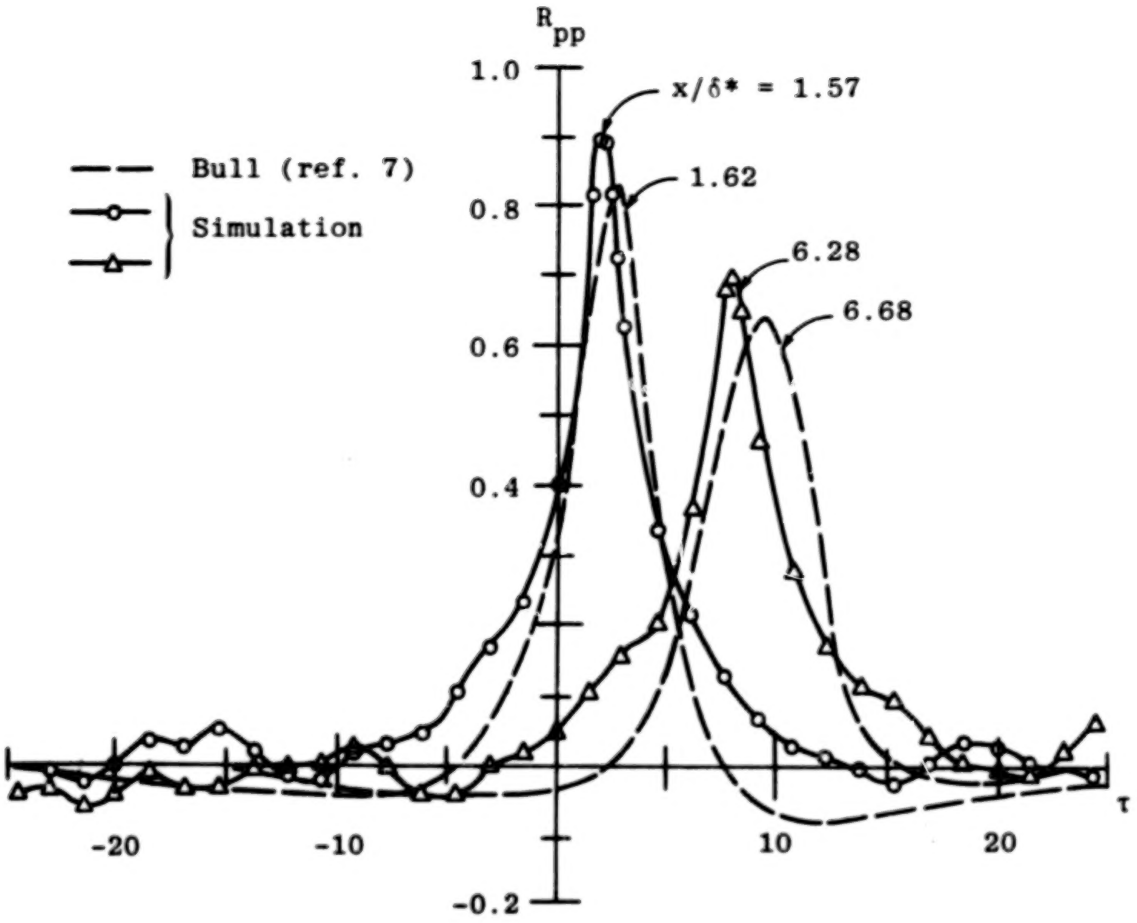


**Figure 7. Space-time correlation for jitter wave simulation.**

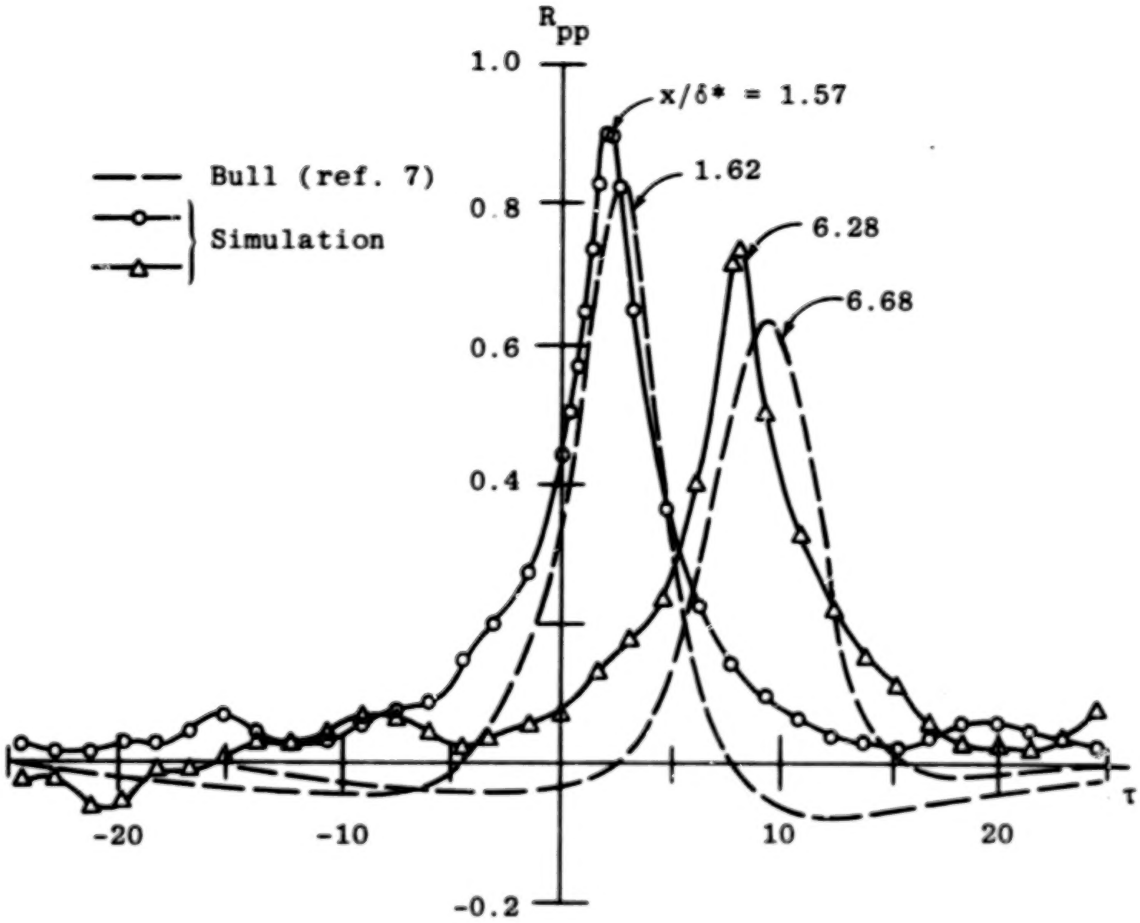


Figure 8. Space-time correlation for skewed wave simulation.

disturbances were convected with different speeds and that their decay was dependent on their characteristic frequencies. As mentioned previously, the constant convection speed may have been high, but since no definitive data were available to permit a reasonable variable convection speed model, the convection speed was not varied. Willmarth and Woolridge (ref. 6) did show the influence of disturbance frequency on decay rate, and it was decided to investigate the influence of frequency-dependent decay on the statistical features of the simulation.

The filtered space-time correlation decay measurements of Willmarth and Woolridge (ref. 6) provide a basis for developing a frequency-dependent decay model, but they are not sufficiently detailed to permit concise modeling. Their low frequency data was taken with a midband Strouhal number of about 0.7 which was more than three times higher than the peak frequency. Their high frequency measurements were centered about a Strouhal number of 5, where the energy level was smaller than the peak level by nearly two orders of magnitude. In addition, since only two frequency bands were employed, there was no way of predicting just how the decay rate varied with frequency.

Decay adjustment with frequency was accomplished by measuring the space-time correlation peak in Willmarth and Woolridge's data at $x/\delta^* = 2.5$. Then, solving the equat on

$$R_{pp}(2.5, \tau_{max}) = 1 - e^{-A\nu/u_\tau x} \tag{8}$$

for A. Using the two frequency levels it was found that

$$A\omega \simeq 5.6 \times 10^6 \frac{1}{\text{sec}} \tag{9}$$

where $\omega$ was the midband radian frequency. Because of the form of the decay parameter in the computer program, decay was related to the disturbance wavelength rather than radian frequency, and a reference value for A. The assumed form was

$$\frac{|p'(\omega, x)|}{|p'(\omega, o)|} = 1 - e^{-3230\ \nu\lambda/(xu_\tau\lambda_r)} \tag{10}$$

where $\lambda_r$ is the wavelength of a reference disturbance, given by

$$\lambda_r = 0.8\ \delta^*\ \gamma \tag{11}$$

with $\gamma$ a parameter (taken as 30 in the test) used to relate the reference disturbance length to a small disturbance length (0.8 $\delta^*$).

A simulation was generated using the linearly dependent frequency (wavelength) decay function given in equation (10). The power spectrum resulting from that simulation is shown in figure 9. It can be seen that frequency-dependent decay has significantly altered the power spectrum. Furthermore, the alteration--particularly at high frequencies--is favorable. Unfortunately, examination of the associated space-time correlation, shown in figure 10, indicates that linearly varying decay has had a devastating effect.

Three significant observations from this study can be made at this point: (1) the double sine wave carrier is clearly superior to the other wave forms examined with regard to producing reasonable space-time correlation curves; (2) wave form does not affect significantly the power spectrum, and the Monte Carlo frequency generating function used thus far does not appear to be acceptable in simulating the power spectrum because of the absence of a clearly defined peak in the energy spectrum; and (3) frequency-dependent decay is a major influence on the shape of both the power spectrum and the space-time correlation curves. These observations permitted a threefold adjustment of the simulation program. Each adjustment will be addressed separately.

### A. Wave Form

The double sine wave disturbance carrier was used for the remainder of the simulations. Its obvious higher harmonic contribution to the wall pressure energy spectrum did not significantly

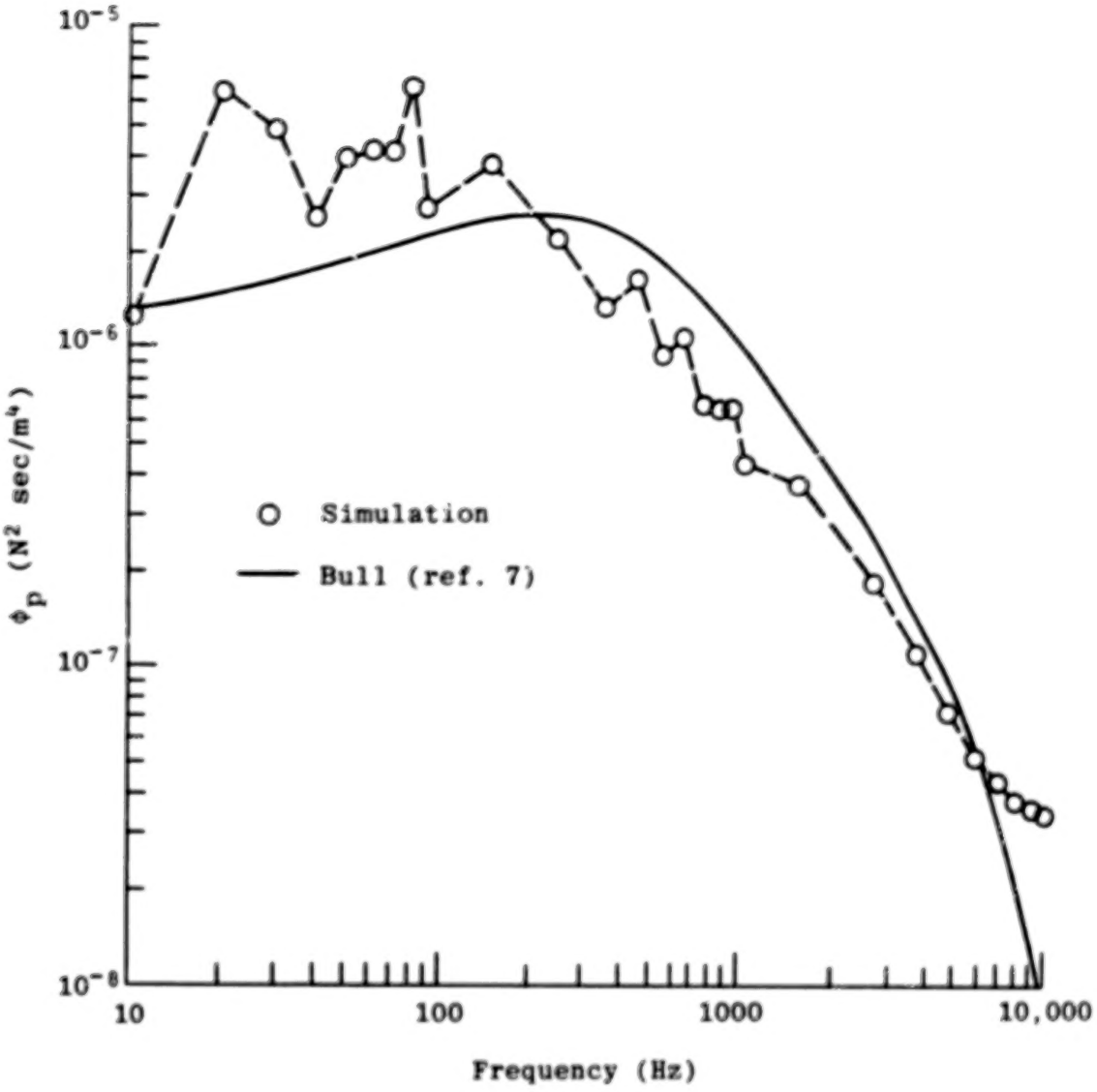


Figure 9. Wall pressure power spectrum for sinusoidal disturbances, decay varying linearly with frequency.

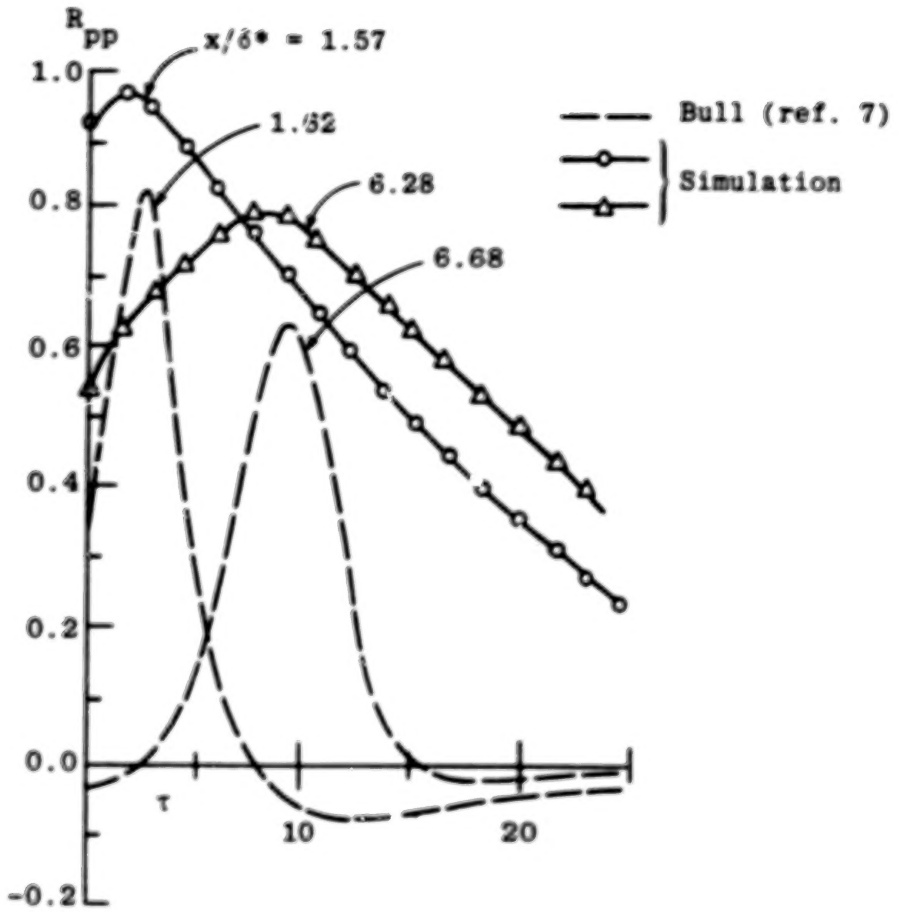


Figure 10. Space-time correlation for sinusoidal waves with decay a linear function of frequency.

alter that spectrum. The fact that different waves nominally with the same shape were not capable of preserving the desired features of the space-time correlation suggests that the higher harmonic aspect of that wave carrier may have physical significance. Regardless of the physical significance, no further wave form studies appeared warranted.

### B. Frequency-Generating Function

An adjustment was certainly required for the Monte Carlo frequency generator. However, it was uncertain at this point just how the combined effects of frequency-dependent decay and a modified frequency generator might interact. Rather than examine the effects separately, the composite spectrum shown in figure 4 was selected as a guide for adjusting the frequency generator and the decay variation, discussed subsequently, was modified simultaneously.

A curve was faired through the simulated spectral data shown in figure 4 and a ratio of desired level (based on Bull's data) to generated level was established. The resulting spectrum, gotten by multiplying the ratio of Bull's values to the simulated values by Bull's original spectrum, is shown in figure 11. Using the resulting spectrum, the cumulative probability function was obtained by graphically integrating the area under the power spectrum curve. That distribution is also shown in figure 11.

Using the features of the cumulative probability distribution function (particularly the upper and lower frequency limit asymptotes) shown in figure 11, the dimensionless frequency-generating function given by

$$\hat{\omega} = 0.523 \left[ \frac{1}{(1 - n)^{.74}} - 1 \right] + 0.799\, n^{2/3} - 0.785\, n \qquad (12)$$

was constructed. No significant deviation between the curve of equation (12) and the curve shown in figure 11 was observed.

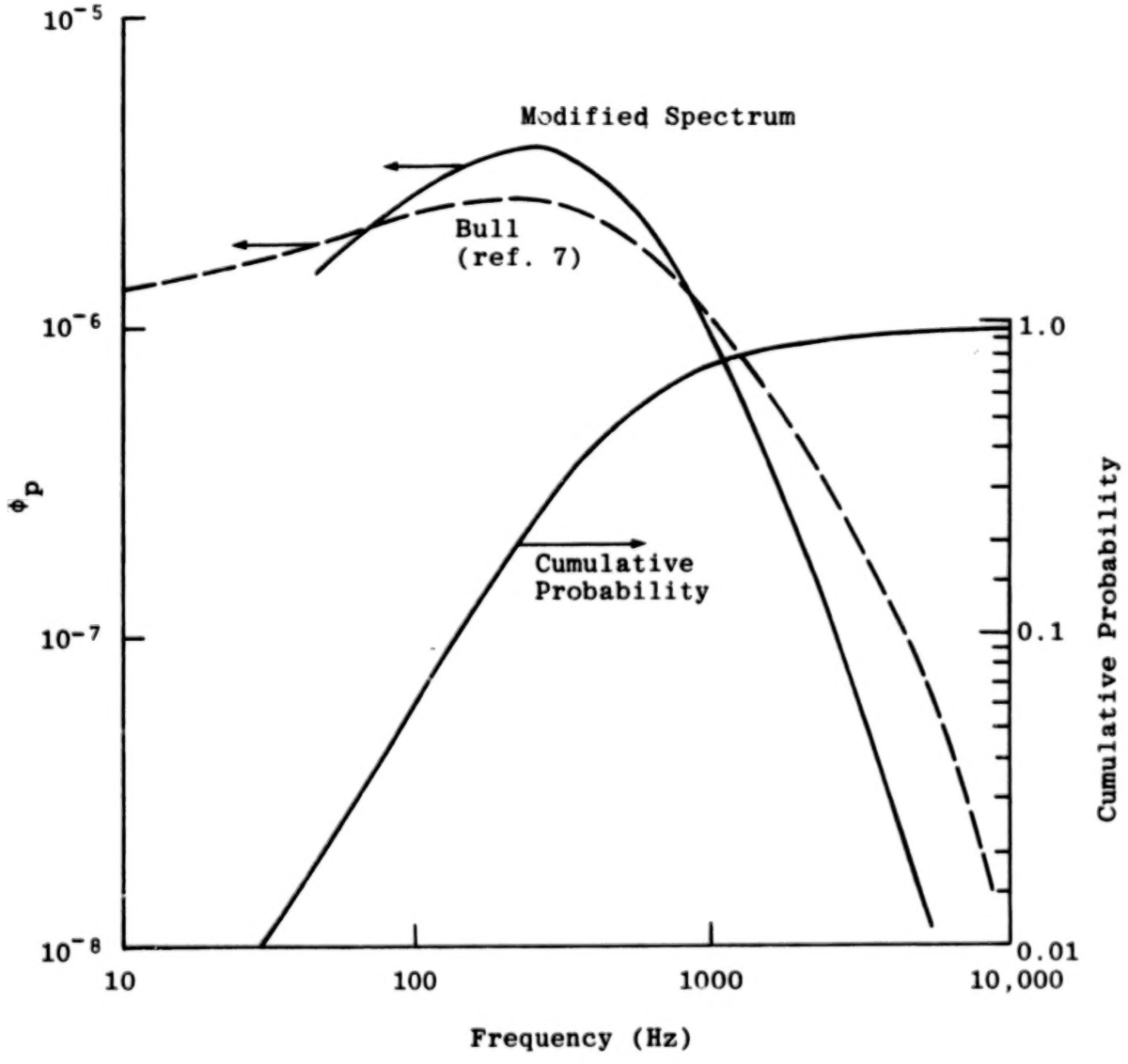


Figure 11. Modified power spectrum and cumulative probability required for frequency generator.

## C. Frequency-Dependent Decay

Based on the drastic effect of frequency-dependent decay on the space-time correlation curves, as shown in figure 10, the linear variation of decay with frequency was abandoned. The difficulty was due to the fact that at the lowest frequencies decay rates were two orders of magnitude slower than at the highest frequencies--causing an inappropriate overemphasis on the low frequency waves and resulting in the greatly widened positive space-time correlation regions shown in figure 10.

Frequency dependent decay was still desirable from the experimental implications, as well as its favorable effect on the power spectrum. An exponentially varying frequency dependent decay function was selected because it was capable of maintaining nearly constant decay rates at the lower frequencies (below Strouhal numbers of about 0.2), while increasing significantly the rate of decay at the higher frequencies. The form used was given by

$$\frac{|p(\omega, x)|}{|p(\omega, 0)|} = 1 - e^{-3000\ \nu\ f(\omega)/(u_\tau x)} \tag{13}$$

where $f(\omega)$ was given by

$$f(\omega) = e^{-(\omega/\omega_o)} = e^{-(\lambda_r/\lambda)} \tag{14}$$

with $\omega_o$ specified in the same manner as $\lambda_r$ in the linear case ($\gamma$ was taken as 10 in this case).

The power spectrum and space-time correlations generated by a simulation using the modifications just described are shown in figures 12 and 13 respectively. Good agreement between the simulation and experimental data is evident. The deviation in decay rate indicated in figure 13 is small (about 10 percent) and can probably be reduced further by adjustments in the decay function. However, the agreement was considered adequate at this point.

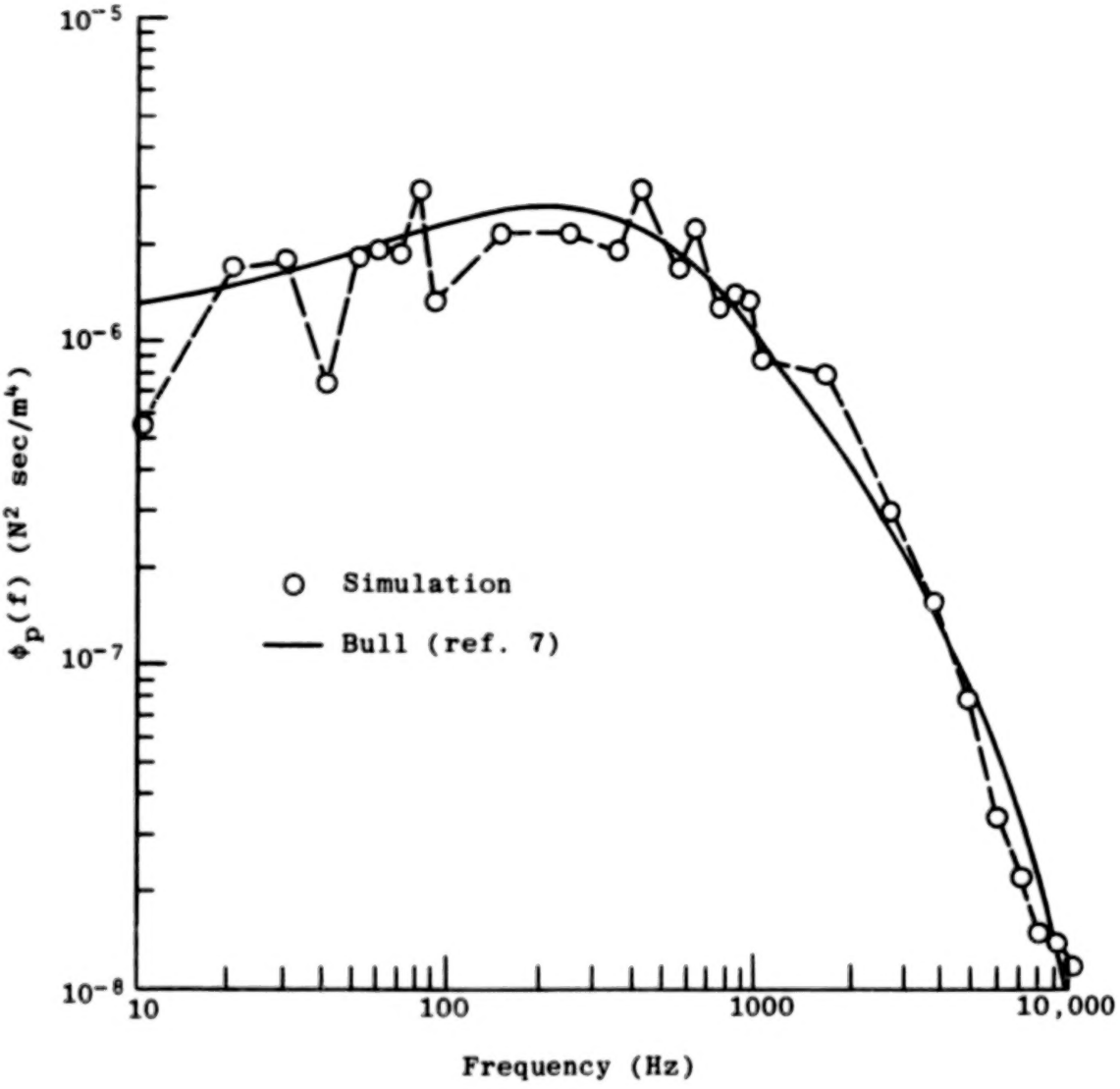


Figure 12. Power spectrum after optimization.

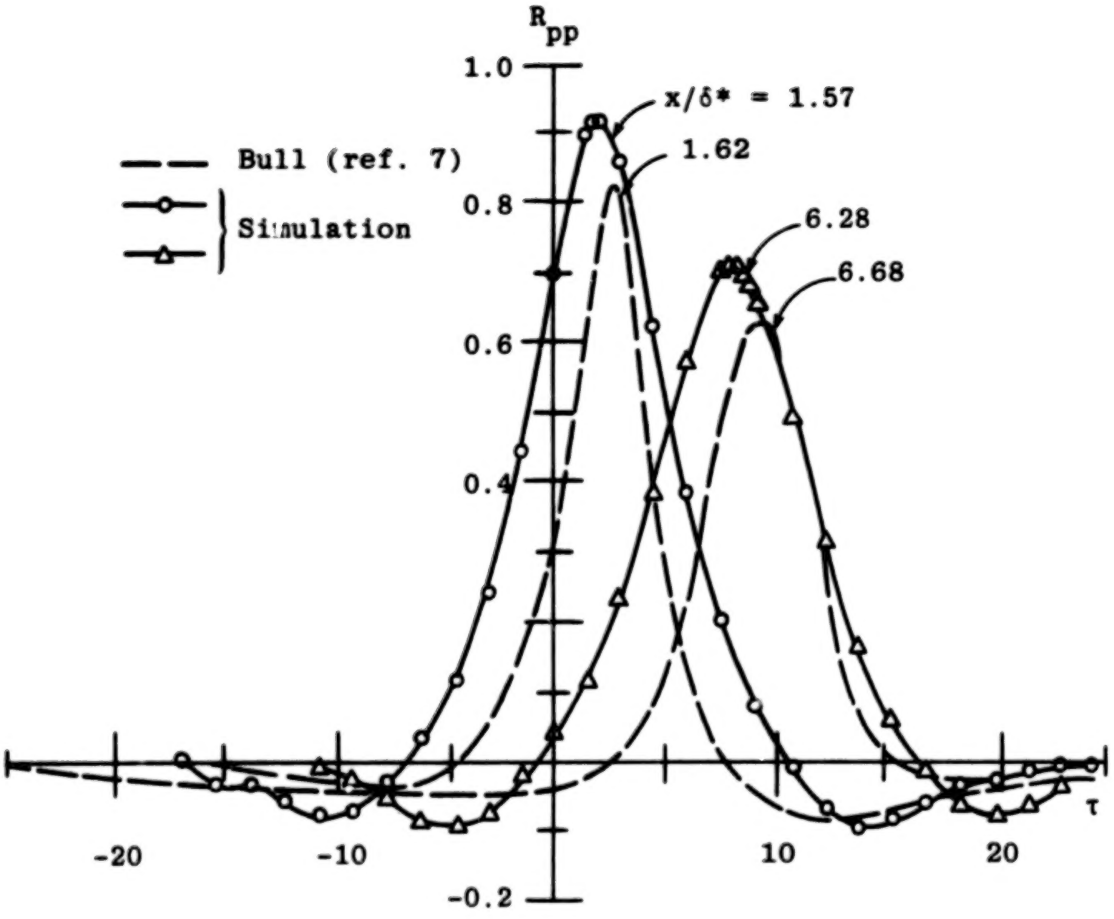


Figure 13. Space-time correlation after optimization.

In concluding this section, it should be noted that no formal discussion of rms pressure level has been made thus far in this report. It is extremely simple to adjust rms pressure level in this simulation because one need only adjust the prefix of the Gaussian amplitude generator. The amplitude of the rms pressure level has no affect on the other statistical properties of the simulation. The desired rms pressure level was assumed to be $3\tau_w$ -- slightly higher than either Bull's (ref. 7) or Willmarth and Woolridge's (ref. 6) measurements, but consistent with the observations of Emmerling (ref. 8) and Bull and Thomas (ref. 9). As evidenced by the comment statement in the computer program listed in the appendix of the present report, a somewhat reduced prefix magnitude (20 percent reduction) was required to yield a nominal $p_{rms}$ of $3\tau_w$ at the five simulation stations. Variations of each of the rms pressure levels from the specified value were about plus or minus five percent.

## IV. RESULTS AND DISCUSSION

This investigation has shown that it is possible to simulate turbulent wall pressure fluctuations using a Monte Carlo approach. The simulation is capable of satisfactorily reproducing rms pressure levels, power spectra, and space-time correlations (in the direction of flow). The simulation permits arbitrary resolution of pressure data in both space and time, making the output directly accessible to other computational analyses.

The latest version of the FORTRAN computer code for generating the simulation is included in the appendix to this report. The space-time correlation calculations generated at the end of the listed simulation program are not correct, but were merely used to check the computation prior to storage on tape. The simulation of 0.767 seconds of pressure data at five spatial locations with a resolution of 46.5 microseconds required nearly 2800 seconds of CDC 6600 computer time.

Obviously, a great deal of computer time is required to generate a simulation. However, generation of a 1 or 2 second simulation

can be used to produce an essentially infinite time simulation simply by randomly accessing segments of the simulation and piecing them together. Since the data is on tape, the simulation output can be read, one time step at a time, into the other computer programs, thereby alleviating the storage requirements for further analyses.

Arbitrary spatial resolution is also limited by the storage capacity of the computer, i.e., pressure data cannot be stored at an infinite number of spatial locations. However, that problem can also be bypassed by taking advantage of the fact that the random number generator in a computer reproduces itself. That is, if the same startup number (seed) is used for all runs and the length of the model does not change (the last storage location must be fixed), the simulation can be repeated. Since the space and time resolution of the output is arbitrary, the computer will go through an identical chain of random numbers and, by changing the storage locations for the output, an arbitrary number of pressure histories for the specified spatial locations can be generated and stored on one or more tapes.

Besides the ability to generate infinite duration one-dimensional pressure histories, a two-dimensional simulation can be produced in much the same manner. If the transverse spacing, $\Delta y$, between storage locations is greater than about 25 $\delta^*$, the same simulation can be randomly accessed to produce pressure histories for successive strips, since $R_{pp}(x, \Delta y, t)$ would be nominally zero. If the spacing is less than 25 $\delta^*$, a similar approach can be used.

When two-dimensional simulations are required where $\Delta y < 25\ \delta^*$, there are a countable number of locations that occupy a strip 25 $\delta^*$ wide. Using the procedure above to lay down histories on the location lines that exceed 25 $\delta^*$, the intermediate strips can be generated by alternately assigning data from the independent strips. The transverse space-time correlation could be used to construct a generating function to yield such a simulation, but further research would be required to augment that case.

Finally, since spatial data scales with $\delta^*$, and time data with $\delta^*/U_\infty$, a given simulation can be used for more than one

flow condition, but the user loses control of space and time resolution of the output, as well as the skin friction coefficient (since $u_\tau/U_\infty$ has already been set in the simulation). The usefulness of a general simulation for all turbulent boundary layers is therefore rather restricted.

The author would like to thank Ramakrishna Balasubramanian for his assistance in constructing the computer codes used in this investigation.

# APPENDIX

## PRESSURE SIMULATION FORTRAN PROGRAM

```
JOB,T,7700,300000,10000.        44677   R4313      101409          BIN,A
USER,BALA,RAMAKRISHNAN                000029300E 37200 NAS          ODU
LINECNT(50000)
REQUEST,TAPE1,HY.          SAVTP,RIL,RSB,PRF1.
REWIND(TAPE1)
RUN(S)
LGO.
-
      PROGRAM SIMU(INPUT,OUTPUT,TAPE5=INPUT,TAPE6=OUTPUT,TAPE1,TAPE2)
      DIMENSION P(5,16500)
      DIMENSION SUMX(8000),SUMY(8000)
      DIMENSION PA(5),PR(5)
      EQUIVALENCE(P(66000),SUMX(1)),(P(74000),SUMY(1))
      NR=5$NW=6
C     NDIM=MAXIMUN TIME DIMENSION
      NDIM=16500
      CDIM=NDIM
C      CORX IS THE ADJUSTMENT FOR DX STREAK.
C           IF MORE THAN ONE BURST PER STREAK, CORX IS NOT UNITY
      CORX=1.
C     CORT IS THE TIME ADJUSTMENT FOR DT-STREAK
      CORT=1.
C     XD=DEVELOPMENT LENGTH (M)
C     XM=MODEL LENGTH (M)
C     PAR IS THE DECAY ADJUSTMENT ACCOUNTING FOR DISTURBANCE SIZE
      PAR=10.
      XD=4.145
      IMJ=0
      XM=0.0
      DXT=0.008
  157  XD=XD+XM
      XT=XD+XM
C     DXT=NODE SPACING ON MODEL(M)
      NXM=5
      XSMX=XD+DXT*NXM
C     XSMX IS THE RIGHT-MOST LOCATION STORING PRESSURE
      US=33.5$BLT=0.0408$UFRIC=1.2587$CNU=0.00001395
      RHO=1.2
      DPT=BLT/8
C     ENTER OTHER DISPLACEMENT THICKNESS HERE IF DESIRED (CM)
C     CALCULATION OF WALL SHEAR STRESS, TW
      TW=RHO*UFRIC*UFRIC
C     CALCULATION OF RMS PRESSURE FLUCTUATION
      PRMS=3.*TW
```

```
C     CALCULATION OF MINIMUM RELEVANT DISTURBANCE LENGTH
C     TWV IS TIME DURATION OF DISTURBANCE
      TWV=DPT/US
C     LENGTH OF SMALL DISTURBANCE
      CLM=0.8*US*TWV
C     DECAY BIAS PARAMETER
      CWV=PAR*CLM
C     MISCELLANEOUS CONSTANTS
      PI=3.1415926
      TPI=2.*PI
      HPI=PI/2.
      C0=2.515517
      C1=0.802853
      C2=0.010328
      D1=1.432788
      D2=0.189269
      D3=0.001308
C     STARTER FOR RANDOM NUMBER GENERATOR
      XSTART=77653.
      RNM=URAN(XSTART)
      XSTART=0.0
C     CALCULATION OF NOMINAL PEAK FREQUENCY
      FPEAK=0.20574*US/(TPI*DPT)
      FMAX=10.*FPEAK
C     COMPATABLE TIME STEP
      DTT=1./FMAX/10.
C     A USER SPECIFIED TIME STEP CAN BE ENTERED HERE
C     THIS TIME STEP IS THE TIME INCREMENT USED IN THE RESOLUTION OF THE
C          OUTPUT--THE INTERNAL FLUCTUATION TIME STEP IS RANDOM
C     MAXIMUM TIME IS CONSTRAINED BY COMPUTER STORAGE.  SET THE NUMBER
C          OF ALLOWABLE TIMESTEPS--NTM
      NTM=16500
C     INITIAL TIME IS TO(SEC)
      TO=0.
      DTAVG=0.
C     PREFIXES FOR RANDOM NUMBER CALCULATIONS
      PX=DPT*UFRIC/US
      PT=DPT/US
      PW=US/DPT
C     CALCULATION OF REQUIRED START UP TIME FOR SIMULATION
      TSO=1.8*XT/US
      NMIN=TSO/DTT
      TMAX1=NMIN*DTT
C     IF NMIN IS GREATER THAN NTM, NTM IS OVERRIDDEN
```

```
      IF(NMIN-NTM)201,201,202
  202 NTM=NMIN
  201 CONTINUE
      TMAX=NTM*DTT
      WRITE(6,100) DTT,TMAX
  100 FORMAT(5X,*DT=*,F10.8,10X,*TMAX=*,F10.4,//)
      TMAXS=CDIM*DTT
      TMAX=TMAX+TMAX1
      NTM2=NDIM-NMIN+2
      TREF=TMAX1
      NREL=0
C     INITIALIZE PRESSURE ARRAY
      DO 52 NX=1,NXM
      DO 52 NT=1,NDIM
   52 P(NX,NT)=0.0
      NFLG=0
      TSUB=0.
C     INITIALIZE LOCATION AND TIME BASE, ETC.
    1 X=0.
      NCT=0
      DTSUM=0.
      TO=TO+DTAVG
      IF(TO-TMAX)12,150,150
  150 IF(NFLG) 151,151,15
  151 NFLG=1
      TMAX1=TMAX
      DO 154 I=1,NXM
      DO 152 J=NMIN,NDIM
      JJ=J+1-NMIN
      P(I,JJ)=P(I,J)
  152 CONTINUE
      DO 153 J=NTM2,NDIM
      P(I,J)=0.0
  153 CONTINUE
  154 CONTINUE
      TSUB=TREF
      TMAXS=TMAXS+TREF
      NREL=NMIN
    2 RNM=URAN(XSTART)
      RNM=0.005+0.99*RNM
C     CALCULATION OF DX USING RANDOM NUMBER RNM
      HP(I)=HP(I)*RNM
      DX=PX*(32.2-2/(RNM+0.619)+72.*RNM**2+0.63*TAN(HP(I)))
      DX=CORX*DX
```

```
      X=X+DX
      RNM=URAN(XSTART)
      RNM=0.005+0.99*RNM
C     CALCULATION OF RADIAN FREQ. FROM NEW RNM
      SRNM=RNM**0.6667
      RRNM=(1.-RNM)**0.74
      FRNM=1./RRNM-1
      W=PW*(0.523*FRNM+0.799*SRNM-0.765*RNM)
      F=W/TP1
      TP=1./F
      DXE=0.8*US*TP
      XO=X-DXE
C     XO IS THE ORIGIN OF THE SINE WAVE FLUCTUATION
C     X IS THE FRONT OF THE SINE WAVE
C     XS IS THE FIRST STATION AT WHICH P IS RECORDED.
C          XS AND NX1 WILL BE TAKEN AS THE FIRST STATION VALUES--THEN OVERIDDEN
      XS=XO
      NX1=1
C     CHECK TO SEE IF THE DISTURBANCE IS OVER THE MODEL
      IF(X-XO)5.5.3
C     IF THE DISTURBANCE IS OVER THE MODEL. HAS IT PASSED THE LAST DATA
C          STATION
    3 IF(X-XSMX)4.1.1
C     NX1 IS THE NUMBER OF THE FIRST STORAGE LOCATION
    4 NX1=(X-XO)/DXT+1.9999
      CXN1=NX1
      XS=XO+CXN1*DXT
    5 CONTINUE
C     GENERATION OF RANDOM TIME STEP
    6 RNM=URAN(XSTART)
      RNM=0.005+0.99*RNM
      HP11=HP1*RNM
      DT=PT*(32.2-2./(RNM+0.619)+72.*RNM**2+0.63*TAN(HP11))
      DT=CORT*DT
      T=TO+DT
      NCT=NCT+1
      DTSUM=DTSUM+DT
      DTAVG=DTSUM/NCT
C     GENERATION OF GAUSSIAN RANDOM PRESSURE AMPLITUDE
      RNM=URAN(XSTART)
      CIND=RNM+0.5
      IND=CIND
      CIND=IND
      PPP=2.*(1.-CIND)-1.
```

```
      ARGR=RNM/(1.+CIND)
      ARG=1./(ARGR*ARGR)
      CT=ALOG(ARG)
      CM=SQRT(CT)
      PMG=CM-(CO+CM*(C1+CM*C2))/(1.+CM*(D1+CM*(D2+CM*D3)))
      XS=XS-DXT
      PE=PRMS*PMG*TMP
C     MODIFICATION OF PRESSURE AMPLITUDE TO ADJUST RMS PRESSURE LEVEL
      PE=0.8*PE
C     DO LOOP FOR STEPPING THROUGH MODEL STORAGE LOCATIONS
      DO 14 NX=NX1,NXM
C     MODEL STATION X-LOCATION
      XS=XS+DXT
C     ARRIVAL TIME OF PRESSURE FLUCTUATION
      DXS=XS-X
      TGO=1.25*DXS/US+T
C     FLUCTUATION DEPARTURE TIME
      DXO=XS-XO
      TSTP=1.25*DXO/US+T
C     DOES TSTP EXCEED TMAX
      IF(TSTP-TMAXS)9,9,7
    7 IF(TGO-TMAXS)8,8,13
    8 NSTOP=NDIM
      GO TO 10
    9 NSTOP=TSTP/DTT
   10 NGO=TGO/DTT
      IF(NGO-NREL)99,99,98
   98 CONTINUE
C     DO LOOP FOR SUCCESSIVE TIME CONTRIBUTIONS TO THE SAME X LOCATION
      DO 12 NT=NGO,NSTOP
      TC=NT*DTT
      THET=TPI*(TC-TGO)/TP
      DELT=TC-T
      XOT=0.8*US*DELT
      IF(XOT-0.0005)19,19,18
   18 CONTINUE
      ARGX=-3000*CNU/(XOT*UFVIC)
C     FREQUENCY DEPENDENT VARIABLE DELAY RATE ADJUSTMENT
      ARGAR=-CWV/DXE
      ARGX=ARGX*EXP(ARGAR)
      DECA=1.-EXP(ARGX)
      GO TO 23
   19 CONTINUE
      DECA=1.
```

```
23  CONTINUE
    DP=PE*SIN(THET)*(1.-COS(THET))
    DP=DP*DELA
    NTIME=NT-NWEL
    P(NX,NTIME)=P(NX,NTIME)+DP
12  CONTINUE
 99 CONTINUE
 13 CONTINUE
 14 CONTINUE
130 FORMAT(5X,F10.5,6E14.6)
    GO TO 2
15  CONTINUE
    NWRT=NTM/8
    CNT=NTM
    DO 11 J=1,5
    PA(J)=0.0
11  PR(J)=0.0
    DO 21 J=1,5
    DO 20 I=1,NTM
    PA(J)=PA(J)+P(J,I)/CNT
    PR(J)=PR(J)+(P(J,I)**2/CNT)
 20  CONTINUE
    PR(J)=PR(J)**0.5
21  CONTINUE
    DO 22 J=1,5
    DO 22 I=1,NTM
22  P(J,I)=P(J,I)-PA(J)
    NYM=1000$NZM=2001
    ANN=2001
    DO 24 KK=1,4
    DO 25 K=1,NYM
    SUM=0.$SUMI=0.
    K1=K-1
    NZ=NZM-K1
    DO 40 M=1,NZ
    SUM=SUM+P(1,M)*P(1,M+K1)/PR(1)**2
    SUMI=SUMI+P(1,M)*P(KK+1,M+K1)/PR(1)/PR(KK+1)
40  CONTINUE
    SUMX(K)=SUM/ANN
    SUMY(K)=SUMI/ANN
25  CONTINUE
    IF(KK.GT.1) GO TO 75
    WRITE(NW,191)
191 FORMAT(1H1)
```

```
      WRITE(NW,200)(SUMX(K),K=1,1000)
  200 FORMAT(5E20.6)
   75 CONTINUE
      WRITE(NW,191)
      WRITE(NW,200)(SUMY(K),K=1,1000)
      NXX=1000
      DO 80 K=1,NXX
      SUM=0.$SUMI=0.
      K1=K-1
      DO 90 M=K,NYM
      SUM=SUM+P(1,M)*P(1,M-K1)/PW(1)**2
      SUMI=SUMI+P(1,M)*P(KK+1,M-K1)/PW(1)/PW(KK+1)
   90 CONTINUE
      SUMX(K)=SUM/ANN
      SUMY(K)=SUMI/ANN
   80 CONTINUE
      IF(KK.GT.1) GO TO 793
      WRITE(NW,191)
      WRITE(NW,200)(SUMX(K),K=1,1000)
  793 CONTINUE
      WRITE(NW,191)
      WRITE(NW,200)(SUMY(K),K=1,1000)
   24 CONTINUE
      JXY=5500
      DO 93 IJJ=1,3
      J1=(IJJ-1)*JXY+1
      J2=IJJ*JXY
      DO 94 KK=1,5
      WRITE(1)(P(KK,JL),JL=J1,J2)
      ENDFILE 1
   94 CONTINUE
   93 CONTINUE
      STOP
      END
```

## REFERENCES


1. Bushnell, D.M., Hefner, J.N., and Ash, R.L.: Compliant wall drag reduction for turbulent boundary layers. Phys. Fluids, vol. **20**, part II, pp. 33-48, 1977.

2. Offen, G.R. and Kline, S.J.: Experiments on the velocity characteristics of 'bursts' and on the interaction between the inner and outer regions of a turbulent boundary layer flow. Thermosciences Division, Mech. Eng. Dept., Stanford University, report no. MD-31, 1973.

3. Praturi, A.K.: Visual study of a turbulent shear flow. Ph.D. dissertation, Dept. Chem. Eng., Ohio State University, 1975.

4. Ash, R.L. and Balasubramanian, R.: Resonance phenomena due to turbulent boundary layer excitation. ASCE Water Resources and Ocean Engineering Convention, San Diego, CA, preprint 2726, April 1976.

5. Willmarth, W.W.: Pressure fluctuations beneath turbulent boundary layers. Ann. Rev. Fluid Mech., vol. 17, pp. 13-38, 1975.

6. Willmarth, W.W. and Woolridge, C.E.: Measurements of the fluctuating pressure at the wall beneath a thick turbulent boundary layer. J. Fluid Mech., vol. 14, pp. 187-210, 1962.

7. Bull, M.K.: Wall pressure fluctuations associated with subsonic turbulent boundary layer flow. J. Fluid Mech., vol. 28, pp. 719-754, 1967.

8. Emmerling, R.: The instantaneous structure of the wall pressure under a turbulent boundary layer flow. Max-Planck-Institut für Strömungsforschung, report no. 9, 1973.

9. Bull, M.K. and Thomas, A.S.W.: High frequency wall pressure fluctuations in turbulent boundary layers. Phys. Fluids, vol. 19, pp. 597-599, 1976.

10. Burton, T.E.: The connection between intermittent turbulent activity near the wall of a turbulent boundary layer with pressure fluctuations at the wall. Mass. Inst. Tech., Dept. of Mech. Eng., report 70208-10 (N75-12258), 1974.

11. Deardorff, J.W.: A numerical study of three-dimensional turbulent channel flow at large Reynolds numbers. J. Fluid Mech., vol. 41, pp. 453-480, 1970.

12. Schumann, U.: Numerical investigation of the wall pressure fluctuations in channel flows. Nuclear Engineering and Design, vol. 32, pp. 37-46, 1976.

13. Ash, R.L.: Simulation of turbulent wall pressure. NASA CR-154872, 1977.

| 1. Report No. | 2. Government Accession No. | 3. Recipient's Catalog No. |
|---|---|---|
| NASA CR-2958 | | |

| 4. Title and Subtitle | 5. Report Date |
|---|---|
| SIMULATION OF TURBULENT WALL PRESSURE | May 1978 |
| | 6. Performing Organization Code |

| 7. Author(s) | 8. Performing Organization Report No. |
|---|---|
| Robert L. Ash | |
| | 10. Work Unit No. |

| 9. Performing Organization Name and Address | 11. Contract or Grant No. |
|---|---|
| Old Dominion University<br>School of Engineering<br>Norfolk, VA 23508 | NSG-1100 |
| | 13. Type of Report and Period Covered |
| 12. Sponsoring Agency Name and Address | Contractor Report |
| National Aeronautics & Space Administration<br>Washington, DC 20546 | 14. Sponsoring Agency Code |

15. Supplementary Notes

Langley Technical Monitor: Jerry N. Hefner

Final Report

16. Abstract

A Monte Carlo procedure has been developed to simulate turbulent boundary layer wall pressure fluctuations. The approach utilizes much of the newly available conditional sampling information to construct the required distribution functions. Various disturbance wave forms have been examined, as well as the effect of frequency-dependent decay. Good agreement between the simulation and experimental data has been achieved for root mean square pressure level, power spectrum, and space-time correlation.

| 17. Key Words (Suggested by Author(s)) | 18. Distribution Statement |
|---|---|
| Turbulent boundary layer<br>Pressure simulation<br>Computational fluid dynamics | Unclassified - Unlimited<br>Subject Category 34 |

| 19. Security Classif. (of this report) | 20. Security Classif. (of this page) | 21. No. of Pages | 22. Price* |
|---|---|---|---|
| Unclassified | Unclassified | 42 | $4.50 |

* For sale by the National Technical Information Service, Springfield, Virginia 22161

NASA-Langley, 1978

# END

9. 19. 78